Visibility enhancement in two-dimensional lensless ghost imaging with true thermal light*

Xi-Hao Chen(陈希浩)[1,†], Ling Yan(燕玲)[1], Wei Wu(吴炜)[1], Shao-Ying Meng(孟少英)[1,‡], Ling-An Wu(吴令安)[2], Zhi-Bin Sun(孙志斌)[3], Chao Wang(王超)[3], and Guang-Jie Zhai(翟光杰)[3]

[1] *Key Laboratory of Optoelectronic Devices and Detection Technology, College of Physics, Liaoning University, Shenyang* 110036, *China*
[2] *Laboratory of Optical Physics, Institute of Physics and Beijing National Laboratory for Condensed Matter Physics, Chinese Academy of Sciences, Beijing* 100190, *China*
[3] *Laboratory of Space Science Experiment Technology, Center for Space Science and Applied Research, Chinese Academy of Sciences, Beijing* 100190, *China*

(Received 17 December 2016; revised manuscript received 14 February 2017; published online 20 April 2017)

We report an experimental demonstration of two-dimensional (2D) lensless ghost imaging with true thermal light. An electrodeless discharge lamp with a higher light intensity than the hollow cathode lamp used before is employed as a light source. The main problem encountered by the 2D lensless ghost imaging with true thermal light is that its coherence time is much shorter than the resolution time of the detection system. To overcome this difficulty we derive a method based on the relationship between the true and measured values of the second-order optical intensity correlation, by which means the visibility of the ghost image can be dramatically enhanced. This method would also be suitable for ghost imaging with natural sunlight.

Keywords: ghost imaging, true thermal light, image visibility, two-dimensional image

PACS: 07.05.Pj, 42.25.Hz, 42.25.Kb **DOI:** 10.1088/1674-1056/26/6/060702

1. Introduction

Ghost imaging (GI) is a new type of optical imaging technique which reconstructs the image of an object by measuring the intensity (photon) correlation of the signals from two light beams, namely the test beam which interacts with the object and the reference beam. Unlike traditional imaging, GI needs a bucket detector without any spatial resolution to collect all the light coming from the object in the test beam, while using a spatially resolving detector, such as a charge-coupled device (CCD), to detect the intensity distribution in the reference beam. The first GI experiment with two-photon entangled light was implemented by Pittman *et al.* in 1995,[1] inspired by the theoretical prediction of Belinskii and Klyshko in 1994.[2] After that, it was found that classical thermal light can also be used to achieve GI.[3–9] So far, GI with thermal light has been investigated at great length in configurations with and without a focusing lens. Moreover, lensless high-order GI has also been realized in efforts to improve the quality of GI.[10–20]

Amongst these GI experiments, various manmade light sources have been employed, including quantum optical,[1] pseudothermal,[4] computer-generated thermal,[21–24] and true thermal light.[7,8] Besides these, sunlight, which is a naturally occurring truly thermal light source,[25] has also been used. To date, most GI experiments have been performed by using pseudothermal light due to the technical difficulties with true thermal GI. The first GI experiment with true thermal light was achieved in a configuration with an imaging lens by Zhang *et al.*,[7] in which a hollow-cathode lamp with high relative intensity and narrow spectrum was chosen as a light source. An indoor experimental demonstration of lensless GI with true thermal light was also performed,[8] where the wavelength used was not the spectral line of Rb but of neon, a buffer gas in the lamp. Later, the most ubiquitous naturally occurring light source, i.e., sunlight, was used to perform an outdoor lensless GI experiment.[25] However, until now ghost images obtained with true thermal light have been cross-sectional or one-dimensional (1D), and have low visibilities, no matter whether an imaging lens is used. Therefore, achieving a 2D image with excellent visibility by using a true thermal light source will be a very important step toward real applications based on GI technology with naturally occurring light such as sunlight.

In this paper, according to our previous work,[7,8] we report a demonstration of lensless 2D GI by using a true thermal light source. We employ a commercial Rb electrodeless discharge lamp (EDL) instead of the hollow-cathode lamp used before as the light source. Because the EDL has a higher light intensity and longer lifetime, the experimental time is greatly shortened so it is easier to obtain a 2D ghost image. However, its coherence time is still very short and estimated to be on the order of about 0.1 ns,[26] which is shorter than the resolution

*Project supported by the National Natural Science Foundation of China (Grant Nos. 11204117, 11304007, and 60907031), the China Postdoctoral Science Foundation (Grant No. 2013M540146), the Fund from the Education Department of Liaoning Province, China (Grant No. L2012001), and the National Hi-Tech Research and Development Program of China (Grant No. 2013AA122902).

†Corresponding author. E-mail: xi-haochen@163.com
‡Corresponding author. E-mail: mengshaoying@163.com

© 2017 Chinese Physical Society and IOP Publishing Ltd

time of the detection systems used in our work. To overcome this difficulty, a new scheme is presented which can greatly enhance the visibility of the image. This method should also be suitable for sunlight GI.

2. Traditional GI

An outline of the experimental setup is shown in Fig. 1. The light from the lamp EDL passes through a monochromator to select out the 780 nm spectral line to form a secondary light source at the monochromator exit; the size of the light source is about 2 mm×2 mm, which is limited by the port slit. A polarizing beamsplitter (PBS) transmits linearly polarized light. The beam is then divided by a 50:50 nonpolarizing beamsplitter (BS). The object, a mask (Obj) consisting of two slits of size 0.8 mm×2.3 mm, 1.6 mm apart, is inserted into the beam reflected from the BS. The single-photon detector APD_1 (SPCM-AQRH-14-FC) can capture all the light passing through the mask by means of the fiber collimator C_1, thus serving as a bucket detector. The transmitted light from the BS is coupled into another single-photon detector APD_2 by the fiber collimator C_2. The receiving area of the collimator, which is limited by a pinhole inserted before C_2, is 300 μm in diameter. The detector output signals are fed into a time-to-amplitude converter (TAC), with detectors APD_1 and APD_2 providing the "start" and "stop" signals, respectively. The TAC output is connected to a multichannel analyzer (MCA), which displays a histogram of the coincidence counts as a function of the difference between the times for the photons to arrive at the two detectors.

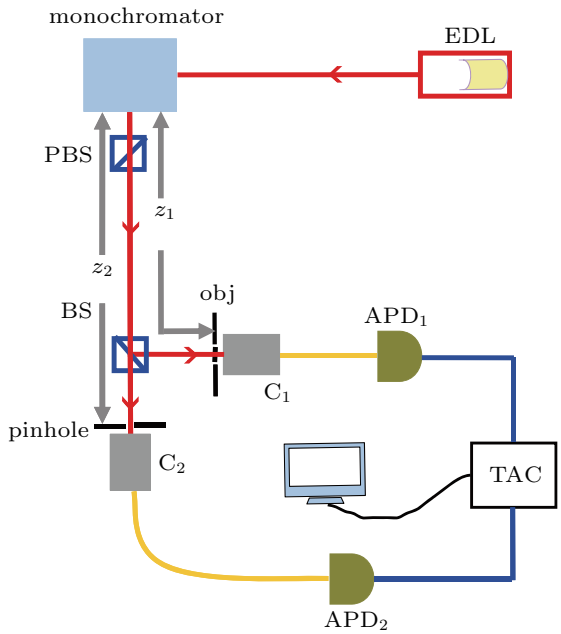


Fig. 1. (color online) Schematic diagram of the experimental setup. EDL, electrodeless discharge lamp; PBS, polarized beamsplitter; BS, beamsplitter; C_i ($i = 1,2$), fiber collimators; APD_i ($i = 1,2$), single-photon detectors. See text for an explanation of other elements.

The transverse normalized second-order correlation function is given by[7,24,25]

$$g^{(2)}(x_2,y_2) \propto 1 + \frac{1}{N}|T(x_2,y_2)|^2, \tag{1}$$

where x_2 and y_2 are the coordinate positions in the transverse plane of fiber collimator C_2, $T(x_2,y_2)$ is the transmission function of the object, and N is the number of transparent features in the object, which is estimated to be equal to about 30 in our scheme.

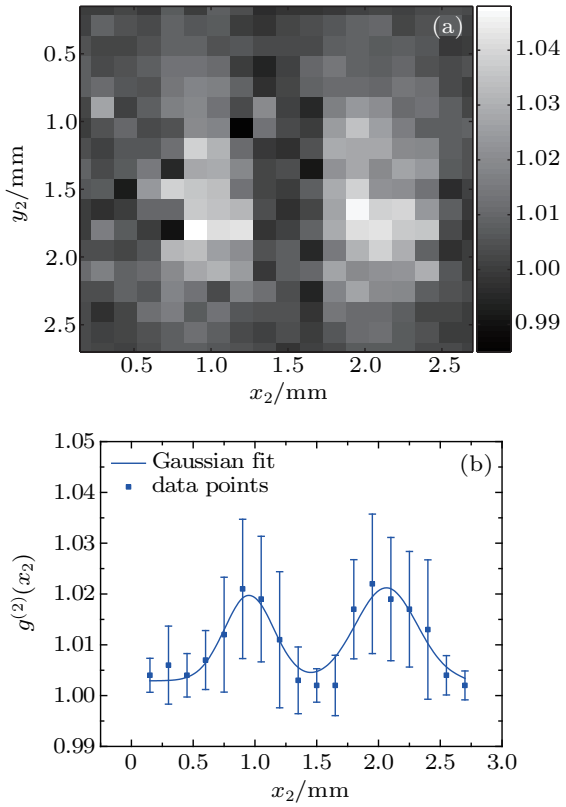


Fig. 2. (color online) Reconstruction of the image of the double-slit. (a) 2D ghost image. (b) Average of 18 horizontal data sections from panel (a).

In our experiment we choose the case where the distance z_1 between the object and effective plane of the lamp is equal to the distance z_2 between the plane of the lamp and the fiber collimator C_2, namely, $z_1 = z_2 = 102$ cm. To image the object, the collimator C_2 together with the pinhole is scanned transversely across the reference beam in steps of 0.15 mm by a 2D motorized translation stage, and the detector coincidence counts are recorded as a function of transverse position x_2 and vertical position y_2 of C_2. The collecting time of the data for each position is more than 20 minutes, which is much shorter than that in our previous experiment due to the higher optical intensity. The normalized second-order correlation function $g^{(2)}(x_2,y_2)$ is calculated as previously, from which we plot the 2D image of the double-slit object over an area of 2.7 mm×2.7 mm (18×18 pixels) as shown in Fig. 2(a). Figure 2(b) shows the corresponding horizontal section, averaged over 18 pixels in the vertical direction. It can be seen

that the visibility of the 2D ghost image is found to be about 1.1%, which is lower than the value of 2.2% that we previously obtained in the 1D imaging experiment[8] and the 5% of the temporal Hanbury Brown–Twiss (HBT) experiment[7] due to the influence of the number of features N mentioned in Eq. (1). This is as expected, since different points on an object will diminish the visibility of the image of other points. Thus the more complicated the object, the worse the visibility will be, as discussed before.[7,8]

However, apart from the factor N in Eq. (1), other reasons for the lower visibility include the limited transverse coherence length of about 0.4 mm in the object plane, the finite area of the fiber collimator C_2, and the short coherence time of the EDL compared with the time jitter of the detection system. In particular, the latter is the uppermost reason for low visibility in true thermal light GI experiments as discussed before,[7,8] and is the main limitation to obtaining good image quality.

3. A new method for visibility enhancement

How to enhance image visibility was discussed by Hanbury Brown in his book many years ago.[27] When the resolution time or time jitter of the detection system is much longer than the coherence time of the thermal source, at zero time delay the relationship between the true and measured values of the temporal second-order correlation function is given by:[27]

$$\begin{aligned} &G_{\mathrm{t}}^{(2)}(\tau=0)-G_{\mathrm{t}}^{(2)}(\tau=\infty) \\ &=\frac{\tau_{\mathrm{s}}}{\tau_0}(G_{\mathrm{m}}^{(2)}(\tau=0)-G_{\mathrm{m}}^{(2)}(\tau=\infty)), \end{aligned} \tag{2}$$

where τ_0 is the coherence time, τ_{s} the resolution time of the detection system, and $G_i^{(2)}(\tau=0)$ the measured ($i=\mathrm{m}$) and true ($i=$ t) value of the second-order correlation function at zero time delay. For an infinite time delay, $G_{\mathrm{t}}^{(2)}(\tau=\infty)$ is the true value of the second-order correlation function and equals $G_{\mathrm{m}}^{(2)}(\tau=\infty)$. In this case there is no longer any correlation because the signals arrive randomly.[28] According to the definition of the normalized second-order correlation function we define the measured value of the normalized second-order correlation function at the moment of zero time delay as

$$g_{\mathrm{m}}^{(2)}(\tau=0)=\frac{G_{\mathrm{m}}^{(2)}(\tau=0)}{G_{\mathrm{m}}^{(2)}(\tau=\infty)}, \tag{3}$$

and substitute it into Eq. (2) to obtain

$$g_{\mathrm{t}}^{(2)}(\tau=0)-1=\frac{\tau_{\mathrm{s}}}{\tau_0}(g_{\mathrm{m}}^{(2)}(\tau=0)-1). \tag{4}$$

Here, $g_{\mathrm{t}}^{(2)}(\tau=0)$ is the true value of the normalized second-order correlation function at zero time delay. To obtain the four parameters in this expression we perform HBT correlation measurements on our thermal light source, then calculate the coherence time $\tau_0=0.1$ ns, the resolution time $\tau_{\mathrm{s}}=1.12$ ns, and $g_{\mathrm{m}}^{(2)}(\tau=0)$ from the experimental data. The results of the temporal HBT experiment are shown on the left scale of Fig. 3, from which we can directly obtain the true value of the normalized second-order intensity correlation function at zero time delay when $\tau_0 \ll \tau_{\mathrm{s}}$. Specifically, from $G_{\mathrm{m}}^{(2)}(\tau)$ in Fig. 3 we can plot $g_{\mathrm{m}}^{(2)}(\tau)$ as shown on the right scale of Fig. 3, in which the full-width-at-half max of the peak is the resolution time of the detection system; the area under the peak is the coherence time according to the equation

$$\tau_0=\int_{-\infty}^{\infty}\left|\Delta g^{(2)}(\tau)\right|^2 \mathrm{d}\tau.$$

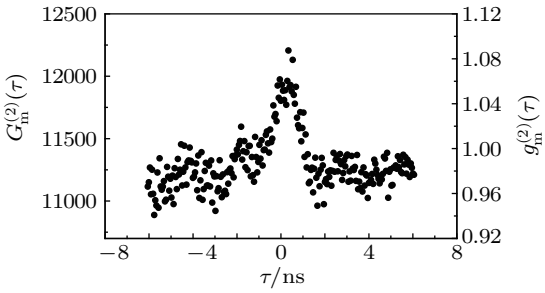


Fig. 3. Coincidence counts $G_{\mathrm{m}}^{(2)}(\tau)$ (left scale) and normalized second-order correlation function $g_{\mathrm{m}}^{(2)}(\tau)$ (right scale) as a function of the arrival-time difference τ between photons at the two detectors.

For each given experimental scheme of GI, τ_0 and τ_{s} are both definite and the same as those of the temporal HBT experiment under the same experimental conditions except that N is involved. However, N is definite for the given GI experimental scheme, too. According to the detection and data processing method, each measured value of the normalized second-order intensity correlation for GI at a given position is obtained by a temporal HBT-like experiment, which is similar to a temporal HBT experiment except that the correlation term is about $1/N$ times (see Eq. (1)), and N lowers the image visibility as mentioned above. However, from the viewpoint of detection, the relationship between the measured and true values in the GI experiment is the same as that between the measured and true values in the temporal HBT experiment. This means that equation (4) is also satisfied in the GI experiment, which can thus be used in the 2D true thermal GI experiment to obtain a high visibility 2D ghost image. Furthermore, in the data processing we set a threshold of $g_{\mathrm{m}}^{(2)}(x_2)=1.01$ to improve the quality of the 2D image, that is to say, we calculate the value of $g_{\mathrm{t}}^{(2)}(x_2)$ when $g_{\mathrm{m}}^{(2)}(x_2)>1.01$; otherwise, we let $g_{\mathrm{t}}^{(2)}(x_2)=g_{\mathrm{m}}^{(2)}(x_2)$. Figure 4(a) presents the 2D ghost image obtained with the same double-slit object, and figure 4(b) shows the corresponding horizontal cross section, averaged over 16 pixels in the vertical direction. The visibility is about 8.9%. It is evident that the visibility is significantly improved compared with Figs. 2(a) and 2(b). Thus, this data

processing method is a powerful means to enhance the visibility when the coherence time of the light source is shorter than the time resolution or jitter of the detection system.

We can know that though the visibility obtained by the new method is about 9 times higher than that of traditional GI, it is much lower than the theoretical value of 1/3 of normalized thermal second-order intensity correlation imaging due to the large N. For demonstrating the effect of N, a spatial HBT-type experiment is taken as an example, which means that $N = 1$. In this case, the relationship between the measured and true values of the normalized second-order optical intensity correlation function are given by[27]

$$g_{\mathrm{t}}^{(2)}(\Delta x) - 1 = \frac{\tau_{\mathrm{s}}}{\tau_0}(g_{\mathrm{m}}^{(2)}(\Delta x) - 1), \tag{5}$$

where $\Delta x = x_2 - x_1$ is the relative difference in position between the two detectors in the x direction.

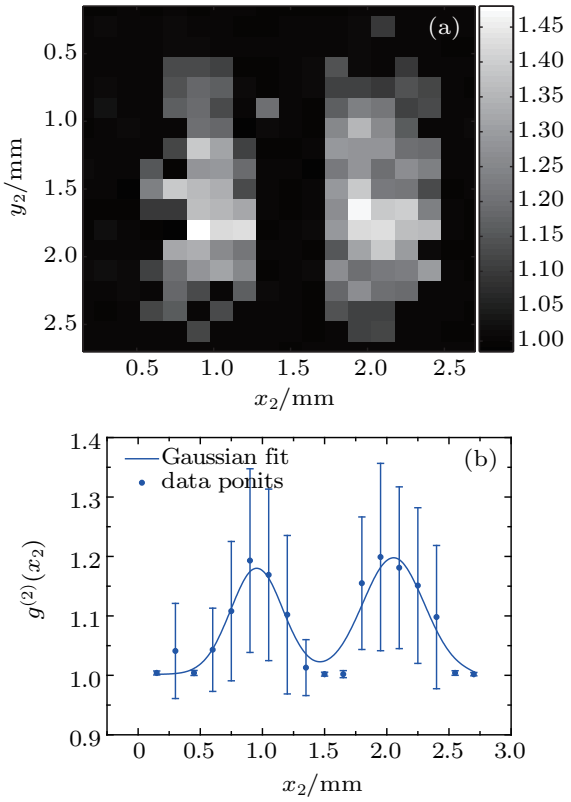


Fig. 4. (color online) Reconstruction of the image of the double-slit. (a) 2D ghost image. (b) Average of 16 horizontal data sections from panel (a). It is evident that the visibilities here are much better than in Fig. 2.

Figure 5 shows the experimental results of the normalized second-order correlation function $g^{(2)}(x_2)$ as a function of relative distance Δx between the two detectors when the position x_1 of APD_1 is taken to be 0. The blue dots denote the measured values of $g^{(2)}(x_2)$ and the red triangles represent the true values according to Eq. (5). It can be seen that the visibility of the true value $g_{\mathrm{t}}^{(2)}(x_2)$ is much better than that of the measured one $g_{\mathrm{m}}^{(2)}(x_2)$. Though the maximum value is still lower than the theoretical value of 2 due to the various factors mentioned above, the visibility is greatly enhanced as predicted. It should be noted that though the main Eqs. (4) and (5) represent a linear relationship between the true and measured values, similar to the case of some general graphic processing methods, they are quite different due to the physical limit to the quantities in these two relations. For example, the value of $g_{\mathrm{t}}^{(2)}(x_2)$ can never be more than 2, which is its theoretical maximum value determined by the statistical properties of thermal light.

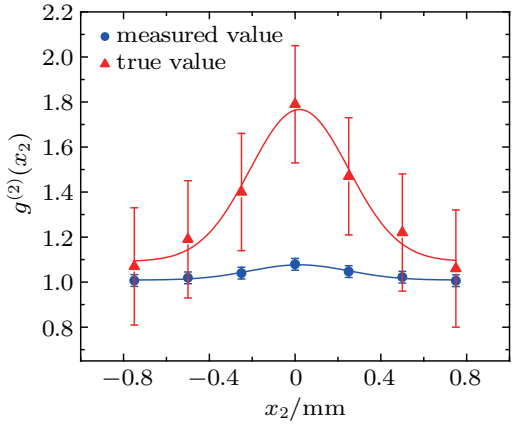


Fig. 5. (color online) Spatial HBT-type experimental results. Blue dots denote the measured values of intensity correlation function $g^{(2)}(x_2)$, red triangles the true values. Solid curves represent Gaussian fits of measured values (blue) and true values (red).

4. Conclusions and perspectives

In this work, we perform a proof-of-principle experiment demonstrating lensless 2D GI with a high intensity EDL as a true thermal light source. To overcome the difficulty that the coherence time of the source is shorter than the time resolution of the detection system, a method derived from the relationship between the true and measured values of the second-order intensity correlation function is introduced. This method can significantly enhance the visibility of the ghost image. Since sunlight GI has similar problems with detection, such a method should also be applicable to obtain better visibility.

References

[1] Pittman T B, Shih Y H, Strekalov D V and Sergienko A V 1995 *Phys. Rev. A* **52** R3429
[2] Belinskii A V and Klyshko D N 1994 *Sov. Phys. JETP* **78** 259
[3] Cheng J and Han S S 2004 *Phys. Rev. Lett.* **92** 093903
[4] Ferri F, Magatti D, Gatti A, Bache M, Brambilla E and Lugiato L A 2005 *Phys. Rev. Lett.* **94** 183602
[5] Cai Y J and Zhu S Y 2005 *Phys. Rev. E* **71** 056607
[6] Cao D Z, Xiong J and Wang K G 2005 *Phys. Rev. A* **71** 013801
[7] Zhang D, Zhai Y H, Wu L A and Chen X H 2005 *Opt. Lett.* **30** 2354
[8] Chen X H, Liu Q, Luo K H and Wu L A 2009 *Opt. Lett.* **34** 695
[9] Valencia A, Scarcelli G, D'Angelo M and Shih Y 2005 *Phys. Rev. Lett.* **94** 063601
[10] Bai Y F and Han S S 2007 *Phys. Rev. A* **76** 043828

[11] Liu Q, Chen X H, Luo K H, Wu W and Wu L A 2009 *Phys. Rev. A* **79** 053844

[12] Agafonov I N, Chekhova M V, Iskhakov T Sh and Penin A N 2008 *Phys. Rev. A* **77** 053801

[13] Cao D Z, Xiong J, Zhang S H, Lin L F, Gao L and Wang K G 2008 *Appl. Phys. Lett.* **92** 201102

[14] Chan K W C, O'Sullivan M N and Boyd R W 2009 *Opt. Lett.* **34** 3343

[15] Chen X H, Agafonov I N, Luo K H, Liu Q, Xian R, Chekhova M V and Wu L A 2010 *Opt. Lett.* **35** 1166

[16] Liu J B and Shih Y H 2009 *Phys. Rev. A* **79** 023819

[17] Zhou Y, Simon J, Liu J B and Shih Y H 2010 *Phys. Rev. A* **81** 043831

[18] Li H, Shi J H, Chen Z P and Zeng G H 2012 *J. Opt. Soc. A* **29** 2256

[19] Chen X H, Chen W, Meng S Y, Wu W, Wu L A and Zhai G J 2013 *J. Opt. Soc. A* **30** 1422

[20] Chen X H, Wu S S, Wu W, Guo W Y, Meng S Y, Sun Z B, Zhai G J, Li M F and Wu L A 2014 *J. Opt. Soc. A* **31** 2105

[21] Shapiro J H 2008 *Phys. Rev. A* **78** 061802

[22] Bromberg Y, Katz O and Silberberg Y 2009 *Phys. Rev. A* **79** 053840

[23] Sun B, Edgar M P, Bowman R, Vittert L E, Welsh S, Bowman A and Padgett M J 2013 *Science* **340** 844

[24] Ferri F, Magatti D, Sala V G and Gatti A 2008 *Appl. Phys. Lett.* **92** 261109

[25] Liu X F, Chen X H, Yao X R, Yu W K, Zhai G J and Wu L A 2014 *Opt. Lett.* **39** 2314

[26] Hanbury Brown R 1974 *The intensity interferometer* (London: Taylor and Francis Ltd.) see Eq. (4.26)

[27] Hanbury Brown R 1974 *The intensity interferometer* (London: Taylor and Francis Ltd.)

[28] Kolobov M I 1999 *Rev. Mod. Phys.* **71** 1539